ingegneria sismica
International Journal of Earthquake Engineering
Anno XXXVIII – Num.1 - 2021

NUMERICAL MODEL FOR DYNAMIC ANALYSIS OF STRUCTURES WITH SEISMIC BASE ISOLATION USING A LAYER OF STONE PEBBLES

Ivan Banović[1], *Jure Radnić*[1], *Nikola Grgić*[1]

[1]University of Split, Faculty of Civil Engineering, Architecture and Geodesy, Split, Croatia

SUMMARY: *This paper presents a numerical model for the dynamic analysis of planar structures with seismic base isolation using a layer of stone pebbles. Following a brief presentation of the previously developed numerical model for structural analysis, the developed constitutive model for the stone pebble layer and the constitutive model for simulating the foundation-isolation layer coupling surface are presented. The model is based on a relatively small number of parameters, some of which were determined experimentally. The numerical model was verified by simulating the performed shake-table tests of simple structural models based on an aseismic layer of stone pebbles, and good agreement between the experimental and numerical results was observed. Finally, further verification and improvement of the presented constitutive models are outlined.*

KEYWORDS: *seismic base isolation, stone pebble layer, numerical model, constitutive model*

1 Introduction

An earthquake is one of the deadliest natural disasters and many countries are located in earthquake-prone regions. Developing countries are more vulnerable to this hazard because people live in areas with high risk of natural disasters (unsafe urban areas). Further, the poor construction of buildings makes them prone to damage in the event of a disaster [Zorn, 2017]. In particular, approximately 60,000 people are killed annually in earthquakes worldwide, with approximately 90% of the deaths occurring in developing countries [OECD, 2008]. For the last 60 years, the application of seismic isolation for earthquake hazard mitigation has been intensively investigated. Various types of base isolators such as elastomeric bearings, lead rubber bearings, rubber bearings, friction pendulum bearings, and dampers [Kelly, 1996] [Naeim and Kelly, 1999] [Lomiento *et al.*, 2013] [Calvi *et al.*, 2016] [Avossa and Pianese, 2017] [Castaldo and Ripani, 2017] [Petrone *et al.*, 2017] [De Domenico, 2019] have been investigated in detail, and have begun to be used regularly in developed countries. In addition, innovative energy dissipation devices based on lattice metamaterials have been proposed [Amendola *et al.*, 2016a] [Amendola *et al.*, 2016b] [Fabbrocino *et al.*, 2016] [Titirla *et al.*, 2017] [Fraternali *et al.*, 2018]. Owing to conventional base isolator limitations (significant installation cost, highly engineered product, and maintenance during use), their application is limited in low-income regions [Tsiavos *et al.*, 2019a]. Therefore, an alternative, simple, low-cost, environmentally friendly, and efficient system for low-income regions is needed [Banović *et al.* 2020a]. One such solution is a seismic base isolation with a unique,

Corresponding author: Ivan Banović, PhD; University of Split, Faculty of Civil Engineering, Architecture and Geodesy, Croatia.
Email: ivan.banovic@gradst.hr

engineered layer below the building foundation for seismic hazard mitigation, known as the geotechnical seismic isolation (GSI) system [Tsang, 2008]. This solution is particularly relevant for developing countries due to its viability and simplicity, with an acceptable reduction of seismic forces on the structure. Some important studies dealing with low-cost seismic isolation are briefly presented below.

The performance of sand and gravel layers for seismic base isolation was tested using shake-table experiments [Teherani and Hasani, 1996] [Anastasopoulos *et al.*, 2012a] [Anastasopoulos *et al.*, 2012b] [Radnić *et. al.*, 2015] [Patil *et al.*, 2016] [Banović *et al.*, 2018a] and numerical studies [Zhao *et al.*, 2016]. More recently, Tsiavos *et al.* [2020a] conducted a large-scale experimental study exploring the beneficial effect of the encapsulation of sand grains between two PVC surfaces on the initiation of sliding and the dissipation of seismic energy between the surfaces. Furthermore, a gravel cushion below a high-rise bridge pier was applied [Pecker *et al.*, 2001] [Pecker *et al.*, 2003] [Steenfelt *et al.*, 2015], with adopted rocking motion as a seismic hazard mitigation technique [Sorrentino *et al.*, 2006] [Sorrentino *et al.*, 2008] [Makris, 2014] [Makris, 2018] [Chung *et al.*, 2019] [Chen *et al.*, 2020].

Tsang [2008] conducted a numerical study on the use of a rubber-soil mixture (RSM) as a low-cost base isolation system, and named it the GSI system. Following this work, numerous researchers have examined the behavior and performance of RSM through several numerical studies [Tsang, 2009] [Mavronicola *et al.*, 2010] [Tsang *et al.*, 2012] [Panjamani *et al.*, 2015] [Bandyopadhyay *et al.*, 2015] [Pitilakis *et al.*, 2015] [Brunet *et al.*, 2016] [Forcellini, 2017] [Tsiavos *et al.*, 2019b] [Tsang and Pitilakis, 2019] [Forcellini, 2020] [Pistolas *et al.*, 2020] [Dhanya *et al.*, 2020] [Hernández *et al.*, 2020] and experimental studies [Xiong and Li, 2013] [Xiong *et al.*, 2014] [Dhanya *et al.*, 2019] [Tsiavos *et al.*, 2019a] [Tsiavos *et al.*, 2020b]. For example, Tsiavos *et al.* [2019a] experimentally tested a sliding layer consisting of a deformable sand-rubber granular mixture as a seismic isolation strategy for low-rise, small-footprint buildings in developing countries. Moreover, Tsang and Pitilakis [2019] developed a simple and efficient lumped-parameter analytical model for analyzing the dynamic soil-foundation-structure interaction of the GSI system.

Kuvat and Sadoglu [2020] proposed asphalt–sand mixtures as an alternative GSI material. The dynamic properties of the geomaterial were investigated by cyclic triaxial experiments. Hadad *et al.* [2017] reported on the seismic performance of kart tires filled with elastomeric recycled materials as base isolators for application in developing countries. The proposed seismic isolators were analyzed via horizontal tests with static and dynamic loadings to determine the horizontal stiffness, hysteretic behavior, and long-term performance. Dhanya *et al.* [2019] proposed the use of geogrid reinforcement to improve the bearing capacity, settlement, and rotational aspects of a shallow foundation resting on a layer of scrap tire–sand mixture under static loading conditions. They reported that the bearing capacity of the layer can be increased up to three times by providing double-layered geogrid reinforcements with a substantial reduction in settlement.

A smooth high-density polyethylene geomembrane as the base isolation material in earthquake hazard mitigation was tested by Yegian and Lahlaf [1992]. Following this work, Yegian and Kadakal [2004] tested various smooth synthetic materials that can serve as seismic protection by absorbing energy through sliding. In particular, Kalpakci *et al.* [2018] tested a UHMWPE geomembrane, based on the study of Yegian and Kadakal [2004]. An artificial soil layer with low shearing resistance, which allows the slipping of the building under the action of strong seismic motions was proposed by Doudoumis *et al.* [2002]. Other interesting applications consist of soil replacement by the thermal insulation layer and geofoam [Murillo *et al.*, 2009] [Azinović *et al.*, 2014] [Azinović *et al.*, 2016] [Koren and Kilar, 2016] [Karatzia *et al.*, 2017] [Azzam *et al.*, 2018].

This paper's authors published several papers [Banović *et al.*, 2018b] [Banović *et al.*, 2019] [Banović *et al.*, 2020a] [Banović *et al.*, 2020b] on the possibility/efficiency of applying a layer of natural stone pebbles under the building foundation for seismic base isolation. First, they reported the results of a preliminary shake-table study [Banović *et al.*, 2018b], where models of stiff and medium-stiff buildings were exposed to four different seismic excitations. The results of the study showed that a layer of pebbles, compared to the rigid base, can significantly reduce the peak acceleration and strains/stresses of the model, with acceptable displacements. Following this work, they started an extensive shake-table campaign to investigate the possibility of using a layer of stone pebbles for the seismic isolation of low-rise buildings in developing countries.

To determine the optimal pebble layer, Banović *et al.* [2019] conducted a shake-table study on the effects of several layer parameters (the layer thickness, the fraction of pebbles, the pebble compaction, the pebble moisture, the vertical contact stress below the foundation, and the effect of repeated excitations) on the layer aseismic efficiency on the sliding rigid block. The following characteristics of the pebble layer were optimal for practical applications: pebble fraction Φ_b = 16-32 mm, pebble layer compaction MS = 30 MPa, and pebble moisture h_m = 10 %. Furthermore, they tested the efficiency of the adopted layer on four models with different stiffnesses [Banović *et al.*, 2020a] and foundation sizes [Banović *et al.*, 2020b], under four different earthquake accelerograms. First, they reported that the efficiency of the considered seismic isolation system decreased with a decrease in model stiffness and that this concept shows great potential for increasing the structural seismic resistance. In addition, compared to the smaller foundation, the larger foundation resulted in a reduced rocking effect, higher earthquake forces, and lower bearing capacity of the tested models, with respectable efficiency (reduced strain/stress, displacement, and increase of the ultimate bearing capacity of the model) for the considered seismic base isolation compared to the foundation on a rigid base.

Although much effort has been invested in recent years in the development of suitable seismic base isolation in developing countries, not enough has been done to develop suitable numerical models to simulate seismic isolation. Some numerical models, whether presented as part of experimental studies or independently, can be found in [Mavronicola *et al.*, 2010] [Tsang, 2012] [Pitilakis *et al.*, 2015] [Brunet *et al.*, 2016] [Zhao *et al.*, 2016].

This paper presents and verifies the developed numerical model for dynamic analysis of planar structures with seismic base isolation using a layer of stone pebbles. The model is an extension of the previously developed numerical model for the dynamic analysis of 2D structures without seismic isolation developed by [Radnić *et al.*, 2011] and later improved by [Radnić *et al.*, 2012] [Baloević *et al.*, 2016a] [Baloević *et al.*, 2016b] [Radnić *et al.*, 2016] [Smilović Zulim *et al.*, 2018] [Baloević *et al.*, 2019] [Smilović Zulim *et al.*, 2019] [Smilović Zulim and Radnić, 2020]. The model is extended with a constitutive material model for simulating the behavior of a stone pebble layer during an earthquake, and modeling the foundation-seismic isolation interaction. The finite element method (FEM) was used for spatial discretization of the structure and isolation layer. In addition to simulating the most important nonlinear effects of individual construction materials (concrete, reinforcement, structural steel, masonry, and pebbles), it is possible to simulate the effect of large

displacements and construction of the structure in stages. The numerical model is based on a small number of parameters, and is primarily intended for practical applications.
The model is verified using shake-table tests of seismically isolated simple models [Banović *et al.*, 2020b] and can be considered reliable. However, further verification is needed.
Section 2 presents a brief overview of the stress state at the top of the aseismic pebble layer below the foundation. The numerical model for the dynamic analysis of 2D structures and the developed constitutive model for the simulation of the aseismic layer are presented in Section 3. Section 4 presents the results of the experimental tests conducted to determine the basic parameters of the constitutive model of the pebble layer. The verification of the presented numerical model using shake-table tests of simple structural models on the aseismic layer is presented in Section 5. Finally, the most important conclusions of the study are presented in Section 6.

2 Mechanical properties of the aseismic layer and stress state at the layer top

Full-scale buildings are most often based on a foundation slab, or the walls and columns are based on individual foundations (so-called strip footing or column footing). Accordingly, the aseismic layer can be constructed on the entire ground floor of the building or below its individual vertical load-bearing elements. The distribution scheme of vertical normal stress σ_v and shear stress τ below the foundation slab or individual foundation on the seismic layer in the planar model is shown in Figure 1. In general, the vertical force N, bending moment M, and shear force Q can be transmitted at the foundation-substrate contact. The distribution of normal and shear stress under the foundation strongly depends on the eccentricity of the vertical force e in relation to the middle of the foundation of length B. If $e = 0$, then the foundation is loaded with a centric compressive force N, which causes vertical compressive stress at the top of the aseismic layer $\sigma_{v,0}$. As M increases, e increases, and the distribution of normal σ_v and shear stress τ below the foundation changes. The vertical tensile stress as well as shear stress, cannot be transmitted in the part where the foundation is lifted from the substrate. The assumed linear σ_v distribution below the foundation is valid only for a rigid foundation with a soft isotropic substrate. The schematically shown τ stress distribution is in accordance with the possibility of shear transmission as a function of σ_v.
With the same axial force N, the maximum compressive stress below the foundation progressively increases with increasing e. For the same force Q, the maximum shear stress also increases progressively. External forces on the foundation are in balance with the resultant force from the stress beneath the foundation.
In earthquake action, the horizontal inertial forces resulting in the transverse force Q can reach a high level relative to force N, depending on the intensity of the earthquake and the dynamic characteristics of the building. Thus, M, resulting from the action of N, can cause a very large e so that N and Q can be transmitted over a very small length of the contact surface of the foundation with substrate b. In this part of the aseismic layer, very large, normal and shear stresses coexist. For $e = B/2$, the foundation overturns, and the stress in the substrate theoretically tends to infinity. During an earthquake, foundation rocking occurs, that is, alternating lifting and rotation of the foundation. As the depth of the aseismic layer increases, stresses σ_v and τ decrease.
The seismic layer under the foundation can be affected simultaneously by large vertical compressive and horizontal shear stresses, which can increase significantly in relation to the

corresponding compressive and shear strengths of the seismic substrate. Therefore, it is necessary to know the actual stress–strain behavior of the aseismic layer and the bearing capacity at different σ_V–τ ratios.

Horizontal normal stress σ_h can also occur in the shallow aseismic layer due to lateral soil resistance and friction between the pebbles and the bottom of the foundation. This stress is significantly smaller than the vertical compressive stress σ_V. The top of the seismic layer is at a very small depth from the top of the surrounding soil, and the lateral soil is regularly significantly deformable. Because of the relatively low level of σ_h in relation to σ_V, its influence on the ultimate bearing capacity of the seismic substrate is ignored here, which is on the side of greater safety.

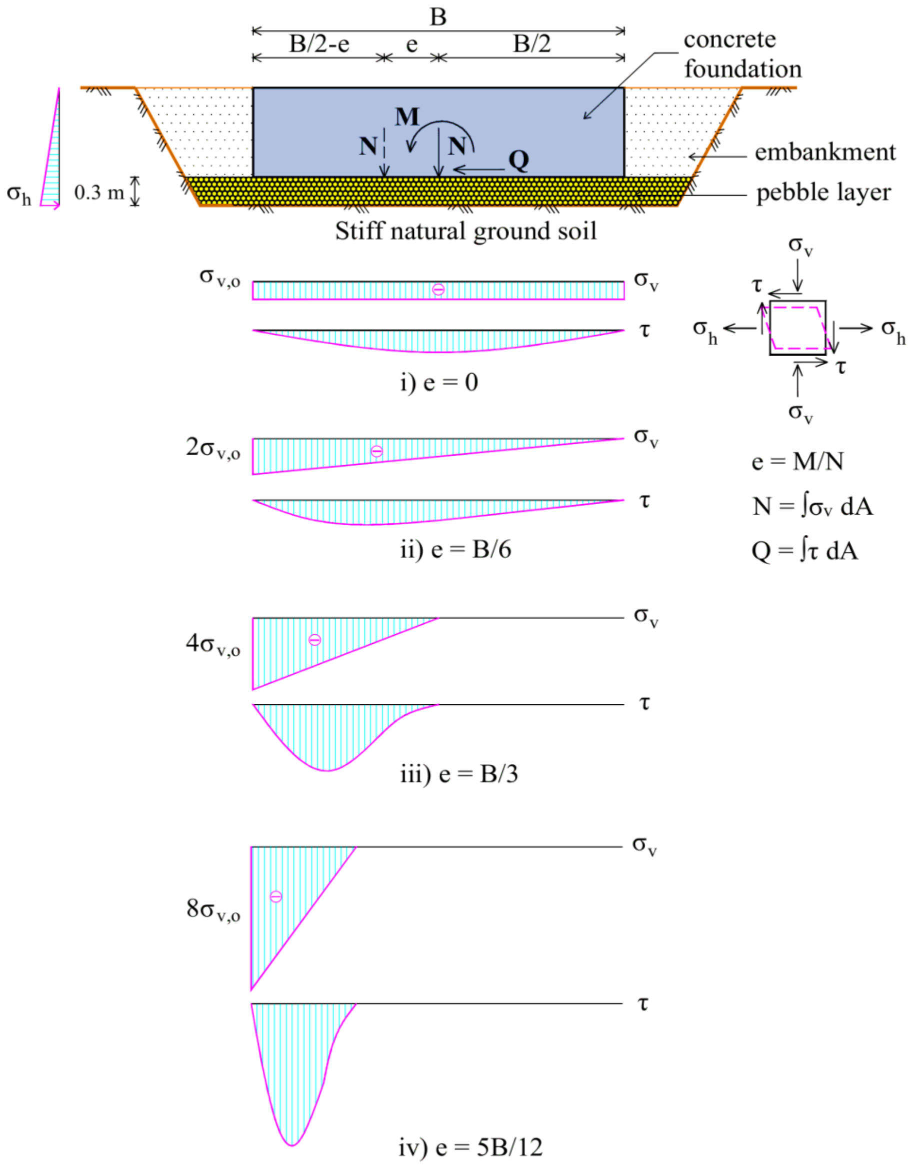

Figure 1 – *Scheme of vertical normal stress and shear-stress distribution below the foundation*

Stone pebbles of fractions 4-8 mm, 8-16 mm, and 16-32 mm [Banović *et al.*, 2019] were tested to determine the optimal layer properties. Based on the performed tests, a fraction of 16-32 mm and a layer thickness of 0.3 m were adopted as optimal (Figure 1). Pebbles are typically granular materials with very complex stress–strain behavior. The behavior of the layer significantly depends on the compaction, which changes under load as well as with the type of applied load. As there is no cohesion between the pebbles, even a well-compacted layer of pebbles has no tensile strength. The pebble layer is anisotropic, with pronounced differences in strength and stiffness/strain in the vertical and horizontal directions. Nevertheless, the strength and modulus of elasticity of the pebble layer in the vertical direction are usually higher than those in the horizontal direction. As with all granular materials, the vertical compressive strength of pebbles is highly dependent on the magnitude of the horizontal lateral pressure. Likewise, the shear strength of the pebble layer strongly depends on the magnitude of the compressive stress. If there is no vertical pressure, the horizontal shear strength of the pebbles disappears.

The following conclusions from previous research need to be highlighted [Banović *et al.*, 2020a] [Banović *et al.*, 2020b]. The presented seismic base isolation is effective only for very stiff and stiff structures based on natural solid ground. For soft structures, as well as for very stiff and stiff structures on soft soil, the isolation is not efficient or even detrimental.

Hence, the presented seismic base isolation using stone pebble layer is effective for buildings with T < 0.3 s - 0.4 s. (where T is the fundamental free oscillation period of the structure without interaction with the ground) and if the substrate on which the isolation is constructed is stiff natural soil (rocky soil, marl, stone, *etc.*).

3 Numerical model

As mentioned in Section 1, the complete numerical model for the dynamic analysis of planar structures with seismic base isolation using a layer of pebbles is coupled with a previously developed and well-tested model for the analysis of structures without seismic isolation. Here, we developed a constitutive model for simulating the behavior of the pebble layer and foundation-pebble layer coupling surface. The most important characteristics of the basic numerical model and the adopted constitutive models for materials (reinforced concrete, steel, and masonry) are briefly described in Section 3.1. The developed constitutive model for stone pebbles is presented in Section 3.2, while the developed constitutive model for the simulation of the foundation-isolation layer coupling surface is presented in Section 3.3.

3.1 Numerical model for dynamic analysis of planar structures

Numerical model for the analysis of planar structures without seismic isolation was developed by [Radnić *et al.*, 2011] and later improved by [Radnić *et al.*, 2012] [Baloević *et al.*, 2016a] [Baloević *et al.*, 2016b] [Radnić *et al.*, 2016] [Smilović Zulim *et al.*, 2018] [Baloević *et al.*, 2019] [Smilović Zulim *et al.*, 2019] [Smilović Zulim and Radnić, 2020]. In this paper, the model will be presented in abbreviated form due to limited space.

FEM was used for spatial discretization of the structure and the isolation layer, assuming a state of plane stress. In addition, it is assumed that the observed system remains a continuum in all phases of deformation. Basic 8-node "serendipity" 2D elements were used to discretize the structure and isolation layer (Figure 2). Further, the reinforcement passing through a 2D element is simulated by a 1D element.

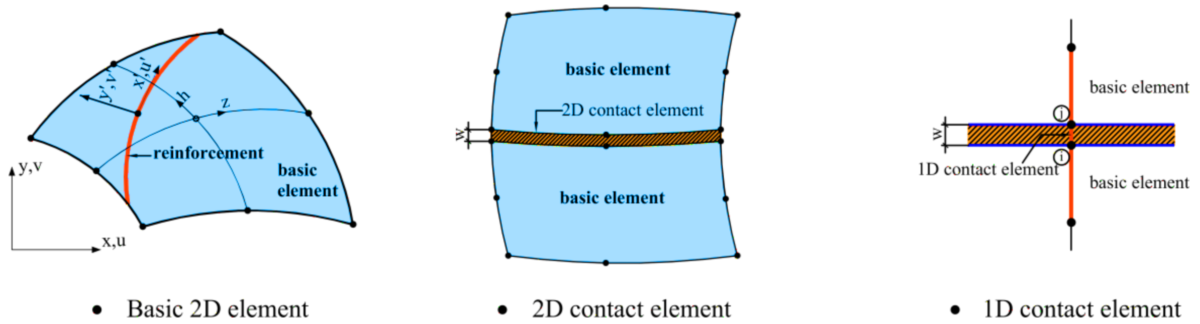

Figure 2 - *Adopted finite elements for spatial discretization [Radnić et al., 2012]*

Contact between basic elements can be simulated with 2D six-node contact finite elements of small thickness. In addition, a 1D bar (two-node) element can simulate possible reinforcement that passes through the contact surface. The sliding, separation, and penetration of the contact surface can be simulated with 2D contact elements.An updated Lagrangian formulation for geometric nonlinear analysis was used. The finite difference method is adopted for temporal discretization, with implicit, explicit, or implicit-explicit Newmark's algorithm, developed in iterative form by Hughes *et al.* [1979] is used for the solution of the dynamic equilibrium equation. Newton-Raphson initial and tangential stiffness methods can be used to solve the system of nonlinear equations. The convergence criterion of the iterative procedure is defined as a function of the increase in displacement increment.
The constitutive model for concrete simulates the nonlinear behavior of concrete in compression and tension (Figure 3). In compression, the elastoplastic behavior with linear unloading behavior is assumed. The yield criterion is defined as a function of stress and the crushing criterion as a function of strain. In tension, elastic behavior is assumed until the uniaxial tensile strength/strain of concrete is reached. Subsequently, the appearance of cracks was assumed.

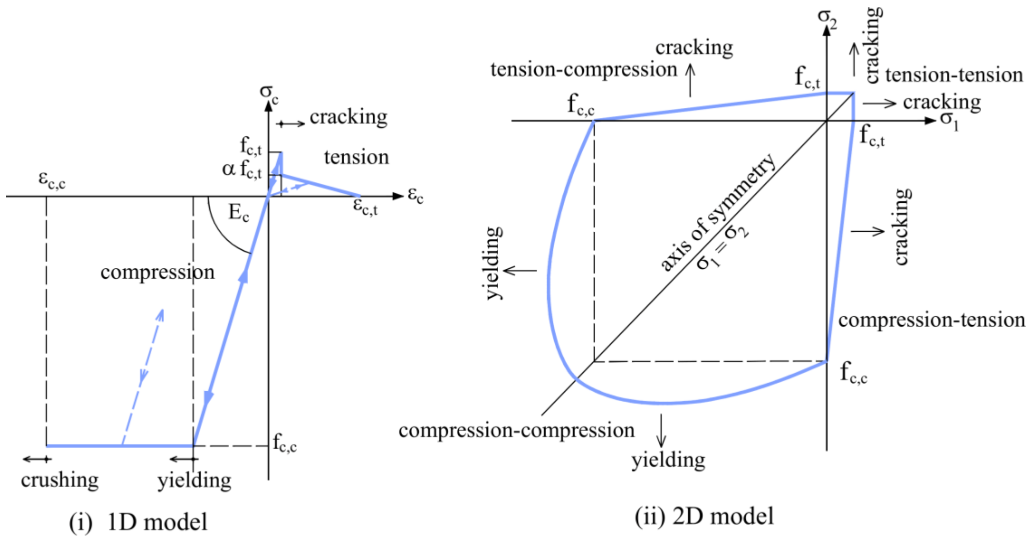

Figure 3 - *Adopted constitutive model for concrete [Radnić et al., 2012]*

The opening and closing of cracks, which were modeled as smeared, was simulated. Possible states of concrete cracks are shown in Figure 4a, and the crack model is shown in Figure 4b. Further, the tensile and shear stiffness of the cracked concrete were modeled (Figure 5). Within a 2D concrete element, the reinforcement is simulated with a 1D bar element. An elastoplastic stress–strain model of reinforcement steel was adopted, with a linear behavior during unloading (Figure 6). The slippage of reinforcement in relation to concrete has not been simulated.

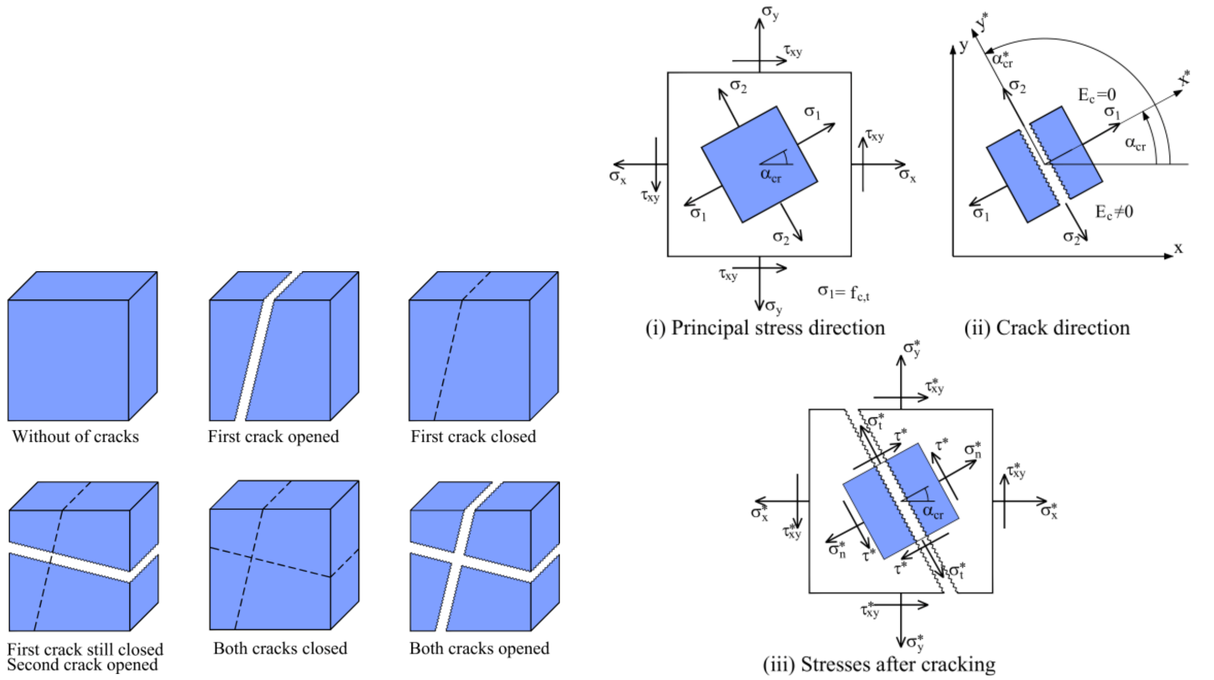

Figure 4 – *Simulation of cracks in concrete [Radnić et al., 2012]: (a) Cracks pattern; (b) Cracks model*

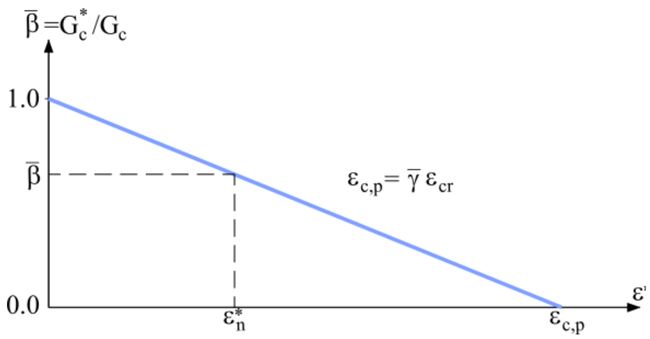

Figure 5 – *Shear stiffness model of the cracked concrete [Radnić et al., 2012]*

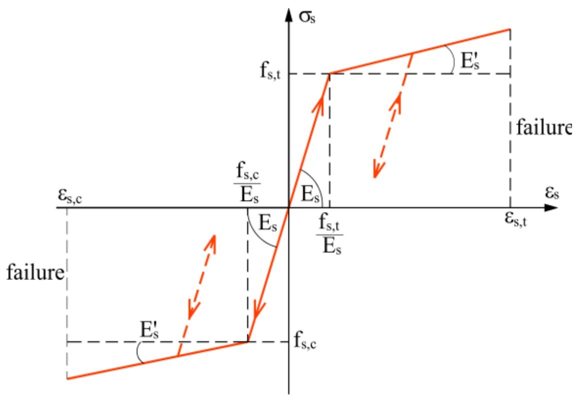

Figure 6 – *Adopted constitutive model for reinforcement [Radnić et al., 2012]*

The constitutive model for masonry is analogous to that for concrete. A macro model of masonry was used, in which the complex interactive behavior of masonry elements and mortar in vertical and horizontal joints was modeled with a representative material of equivalent properties.
This approach allows the use of larger finite elements, as well as simpler and faster analyses. It is possible to use an isotropic or orthotropic model of masonry behavior. The orthotropic behavior model allows analyses with different load-bearing and stiffness parameters in the vertical and horizontal directions (Figure 7). The effect of biaxial compressive stresses on the limit bearing capacity of masonry has not been modeled.
Crack model for masonry is analogous to the crack model for concrete (Figure 4). The collapse of the masonry due to the shear stress in the horizontal plane is modelled (Figure 8). The shear stiffness of cracked masonry is modeled similar as for concrete (Figure 9).
The behavior of structural steel is simulated by an elastoplastic constitutive model in compression and tension (Figure 10). The Von Mises yield criterion is defined as a function of stress, and the failure criterion as a function of strain. Linear behavior was adopted during unloading.

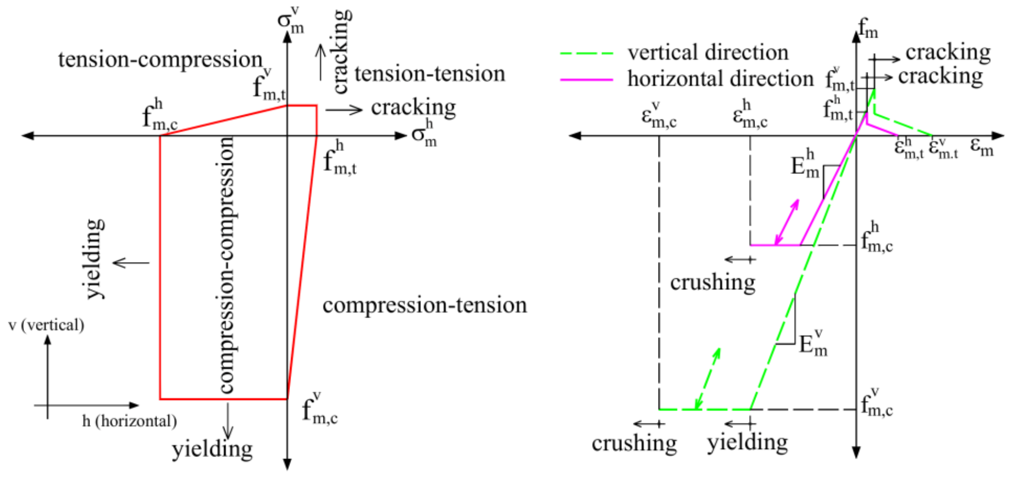

(i) 2D model (ii) 1D model

Figure 7 - *Adopted orthotropic constitutive model for masonry [Radnić et al., 2012]*

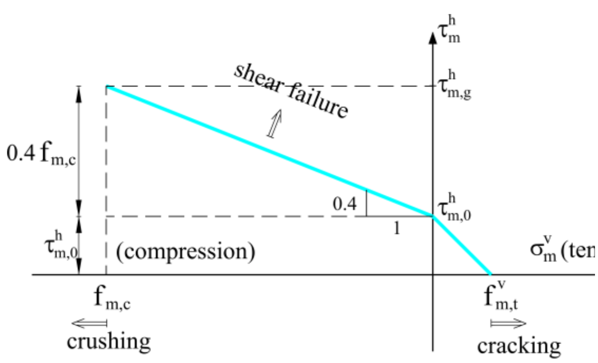

Figure 8 – *Shear failure of masonry [Radnić et al., 2012]*

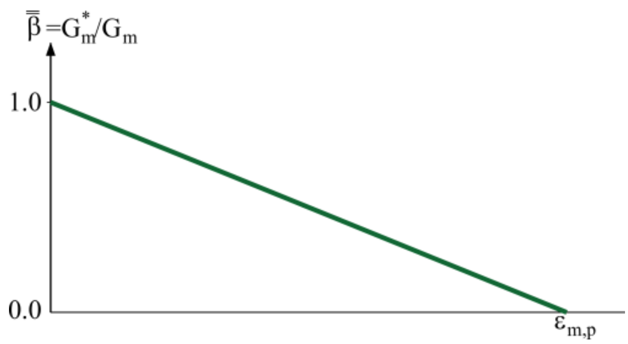

Figure 9 – *Shear stiffness of cracked masonry [Radnić et al., 2012]*

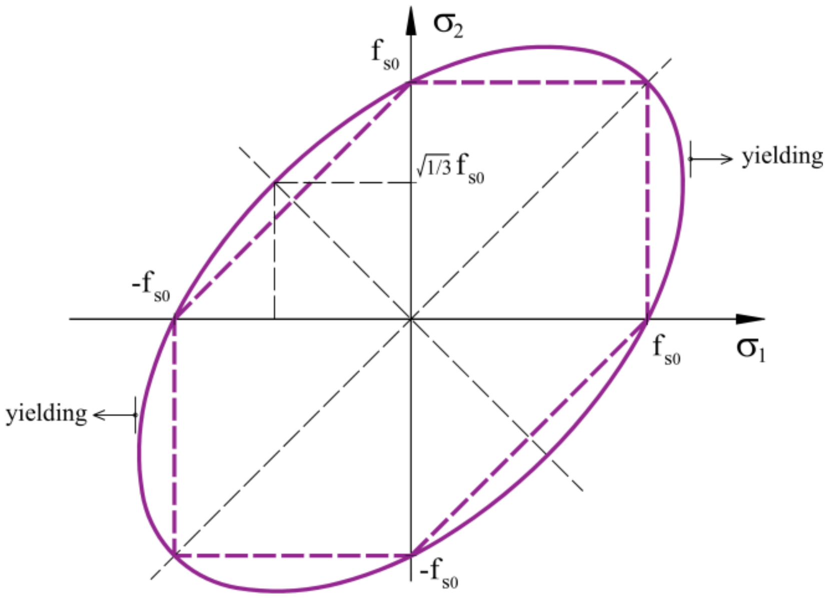

Figure 10 - *Adopted steel constitutive model [Baloević et al., 2016a]*

3.2 The constitutive model for stone pebble layer

The complex behavior of this granular material is described by the simplified constitutive model shown in Figure 11, and is intended for engineering applications in practice. The pebble layer is modeled as a homogeneous orthotropic elastoplastic material, where the main directions of anisotropy are vertical (*v*) and horizontal (*h*).

Figure 11 presents the adopted relation between normal vertical and horizontal stresses and strains, separately for 1D-presentation and 2D-presentation. Symbols in the figure denote the following: σ_v, σ_h normal vertical and horizontal stress; ε_v, ε_h normal strains; f_v, f_h compressive strengths; E_v, E_h modulus of elasticity; $\varepsilon_{e,v}$, $\varepsilon_{e,h}$ yield strains; $\varepsilon_{u,v}$, $\varepsilon_{u,h}$ limit compressive strains. As can be seen from Figure 11, it was assumed that pebbles could only transmit compressive stress. In addition, the influence of lateral pressure on the vertical strength of the pebbles is not included. It should be noted that the possible lateral pressure in a thin layer of pebbles is usually very small. Thus, the linear–elastic behavior in compression is assumed until the compressive strength f_v, f_h is attained, that is, the yield strains $\varepsilon_{e,v}$, $\varepsilon_{e,h}$ are attained, respectively. After the yield criterion has been satisfied, an ideal plastic behavior is adopted. The pebble crushing criterion is defined by the limit compressive strains $\varepsilon_{u,v}$, $\varepsilon_{u,h}$. Linear behavior was adopted during unloading. As the pebbles were treated as a homogeneous continuum, the opening of the cracks in tension and their closing in compression were monitored. It should be noted that these cracks are fictitious, that is, they simulate the pebble displacement under tension stress. A model of fixed distributed cracks was adopted, which was modeled as for concrete and masonry [Radnić *et al.*, 2012]. Assuming elastic behavior, Equation (1) and Equation (2) apply:

$$\varepsilon_{e,v} = f_v / E_v \tag{1}$$

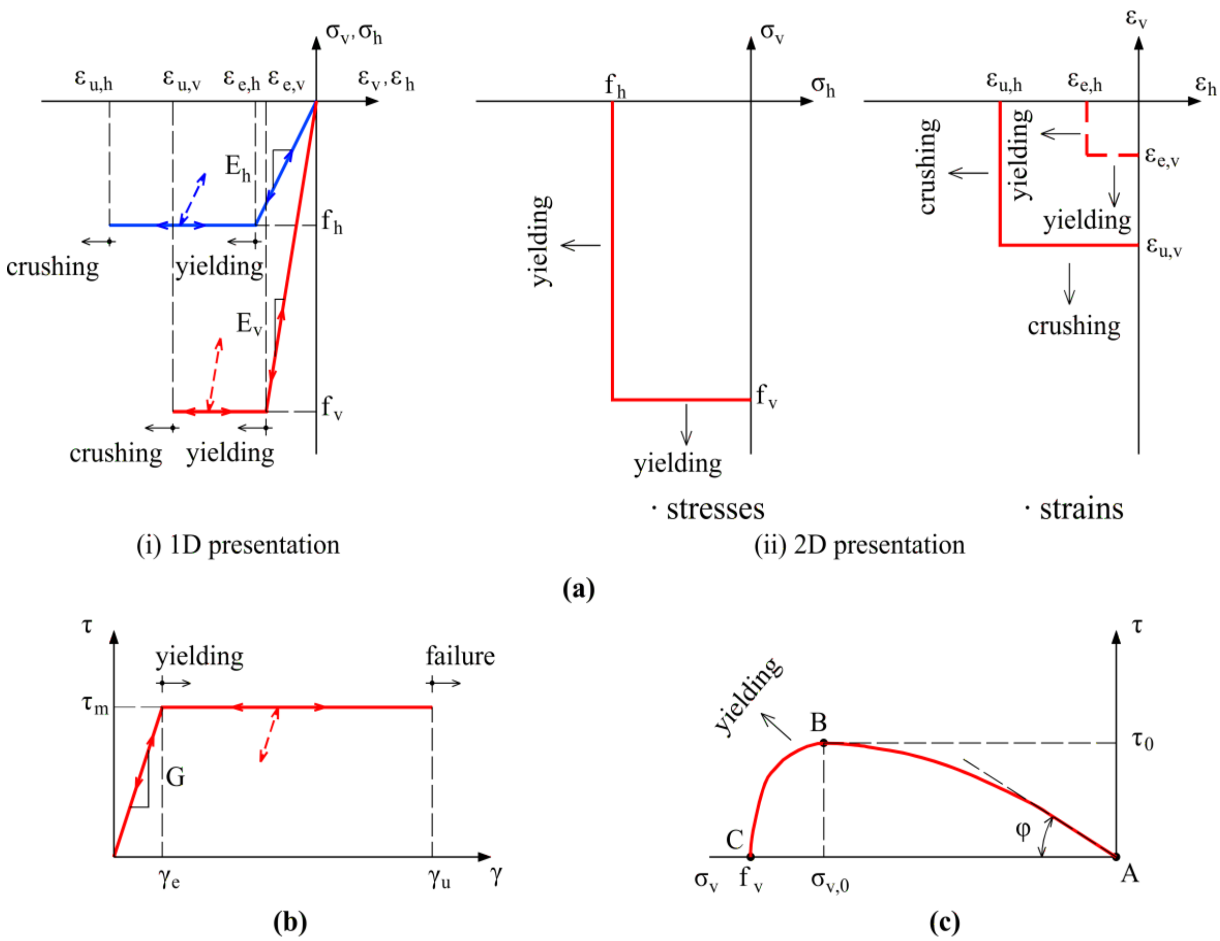

Figure 11 - *Adopted constitutive model for stone pebbles: (a) Normal stress-normal strain relation; (b) Shear stress-shear strain relation; (c) Shear strength-normal stress relation*

$$\varepsilon_{e,h} = f_h / E_h \tag{2}$$

The orthotropic coefficient c_0 is defined by:

$$c_0 = E_h / E_v = f_h / f_v \tag{3}$$

Wherein valid:

$$E_h \cdot \nu_h = E_v \cdot \nu_v \tag{4}$$

$$c_0 = \nu_v / \nu_h \tag{5}$$

where ν_h and ν_v are Poisson's ratios for the horizontal and vertical directions, respectively. The relationship between shear stress τ and shear strain γ is presented in Figure 11. An elastoplastic relation is also assumed. Symbols in the Figure have the following meaning: τ_m

shear strength, G shear modulus, $\gamma_e = \tau_m / G$ yield shear strain, and γ_u limit shear strain. Linear behavior was adopted during unloading. In shear, the yield criterion is also defined as a function of stress, and the crushing criterion as a function of strain, analogously adopted for normal stress.
The shear modulus of pebbles G is defined by:

$$G = 1 / [(1+\nu_h)/E_h + (1+\nu_v)/E_v] \tag{6}$$

Further, the shear stress-normal stress relation for pebbles is also presented in Figure 11. The relation τ-σ_v is approximated by a cubic parabola passing through points A, B, and C. Symbols in the Figure have the following meaning: φ pebble friction angle, and $\sigma_{v,0}$ vertical compressive stress at which the maximum shear strength of the pebbles τ_0 is achieved. Thus, the tangent to the stress–strain curve at point A is at an angle φ, while at point B, the tangent of the curve is horizontal. In the lack of experimental data, $\sigma_{v,0}=0.8 f_v$ and $\tau_0=0.3 f_v$ is assumed in this study. Thus, if the ratio τ-σ_v is such that it is below the assumed curve, the shear bearing capacity criterion is satisfied. Otherwise, “the current” shear stress τ is reduced to the curve for “the current” σ_v and a further iterative procedure is performed with $G = 0$ (plastic yielding). The shear failure criterion for that point is defined when $\gamma > \gamma_u$.

3.3 Constitutive model for simulation of foundation-pebble layer coupling surface behavior

2D six-node contact finite elements were used to simulate the foundation-pebble layer coupling surface. Contact elements can transmit compressive normal and shear stresses. The constitutive model for these elements is presented in Figure 12. The normal stress–normal strain relation for the contact element $\sigma_{v,c}$- $\varepsilon_{v,c}$ (Figure 12) is identical to that for the pebble layer (Figure 12). Further, the shear stress–shear strain relation (Figure 12) is analogous to that in Figure 12, where the values of $\tau_{m,c}$, $\gamma_{u,c}$, $\gamma_{e,c}$ depend on the foundation surface roughness, that is, the foundation construction technology.
In the previously performed experiments [Banović *et al.*, 2018b] [Banović *et al.*, 2020a] [Banović *et al.*, 2020b], the foundation of the model was prefabricated with a smooth bottom surface. Therefore, the above values are lower than those in Figure 11. If the foundation was to be concreted on site, directly at the top of the pebble layer into which the concrete would penetrate, the stated values $\tau_{m,c}$, $\gamma_{u,c}$, $\gamma_{e,c}$ would be larger than the corresponding ones within the pebble layer. In this case, the above-mentioned parameters can be adopted for the pebble layer because the thickness of the contact element is very small.
The adopted model of the shear strength of the contact elements is shown in Figure 12. It is analogous to that in Figure 11, that is, following the above stated on the influence of the foundation surface roughness. In the case of concreting the foundation on site, it can be assumed that $\tau_{0,c}$, φ_c are equal to τ_0, φ, respectively. In the case of a smooth bottom surface of the foundation, $\tau_{0,c}$, φ_c has a lower value than τ_0, φ.

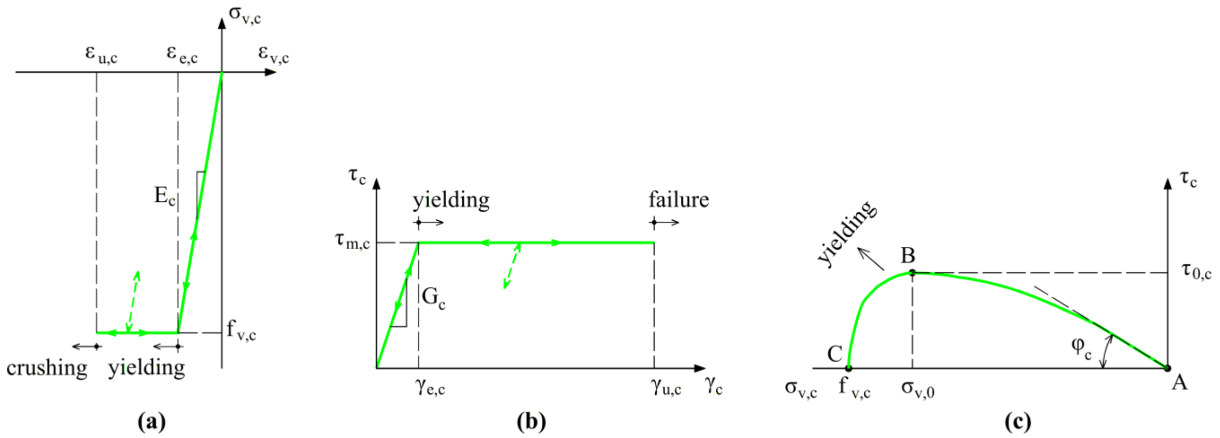

Figure 12 – *Adopted constitutive model for foundation-pebble layer coupling surface: (a) Normal stress–normal strain relation; (b) Shear strength–shear strain relation; (c) Shear stress–normal stress relation*

4 Experimental tests for determining the parameters of the pebble layer and foundation-pebble layer coupling surface constitutive models

A limited number of experimental tests to determine the main parameters of the presented constitutive model of pebbles and the constitutive model of the foundation-pebble layer coupling surface were performed. More extensive experimental tests and improvement of the pebble layer constitutive model for the influence of different levels of horizontal stress are planned to continue urgently.

4.1 Some parameters of the pebble layer

The shear strength of the pebble layer for constant levels of vertical effective stress was determined using a large-scale direct shear test. For the constant σ_v stress state, the shear stress–shear displacement (strain) relation was determined through continuous monitoring of the horizontal shear force until the shear failure of the sample. The shear strength of the sample was determined for a wide σ_v spectrum, ranging from 50 kPa to 600 kPa. Based on the normal stress–shear stress relation, the friction angle φ of the pebbles was determined.

In addition to the classic direct shear test, the pebbles were tested only for vertical stress, without applying a horizontal force. Testing was performed in a direct shear box, and a normal stress–normal strain curve was derived. The vertical strains of the pebbles were calculated based on the measured vertical displacement. Further, based on the measured horizontal strains of the metal shear box, the horizontal stress of the pebbles was calculated.

Based on these data, the initial modulus of elasticity in the vertical and horizontal directions and Poisson’s ratios for the horizontal direction were calculated. In addition, the bulk density of the pebbles was measured.

Basic data on the apparatus used to perform the direct shear test are shown in Figure 13. Two horizontally fixed and middle horizontally movable metal square shear boxes, with internal dimensions of 300 mm × 300 mm and height of 120 mm, were used.

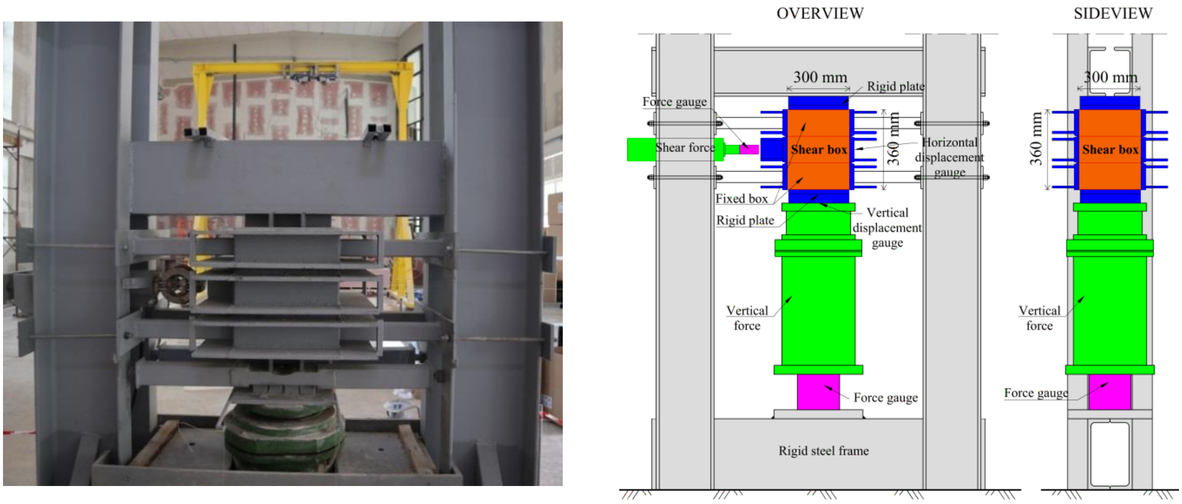

(a) (b)

Figure 13 – *Large-scale direct shear apparatus: (a) Photography of experimental setup, (b) Basic data of the adopted setup*

Shear boxes are formed from welded steel sheets and provide extremely small lateral displacements/strains even for very high vertical pebble stresses. It can be concluded that for vertical loading, the pebbles are in a stress–strain state of vertical stress with prevented horizontal strain. Prior to performing each test, the pebbles were first loaded with a vertical force to ensure compaction MS = 30 MPa. After maintaining a constant vertical force for 15 min, the sample was unloaded and then loaded with vertical force to the level of the considered constant σ_v. After maintaining the designed stress σ_v for 10 min, a horizontal shear force was applied until the shear failure of the pebble sample.

The measured quantities during the direct shear testing are presented in Figure 14. The vertical force V, horizontal force H, displacements v, u, and strain ε_I were measured.

As stated above, prior direct shear tests, the pebbles were tested only with vertical stress, without applying a horizontal force. Normal stress–normal strain curve derived from that test is presented in Figure 15. The relationship between the vertical stress σ_v and the average vertical strain of the pebbles $\varepsilon_v = v/h$ over the entire height of the specimen h = 300 mm for vertical stress is presented in Figure 15. The stress was calculated in relation to the initial shear box area, which remained unchanged with increasing force V.

With the exception of the initial part of the diagram, where the "adjustment" at the initial load of the pebbles occurs, the behavior at low vertical compressive stress is almost linear. The average modulus of elasticity of the pebbles in the vertical direction is E_v = 270 MPa. As the normal stress increases, the normal stress–normal strain curve becomes increasingly nonlinear and the tangent modulus of elasticity E_v decreases. However, it should be noted that even under such a low σ_v horizontal lateral compressive stress σ_h occurs on the pebbles because of the prevented lateral strain of the shear box. Based on the measured lateral strain of the box for $\sigma_v = 0.5$ MPa, it is estimated that the shear box opposes the approximate horizontal lateral pressure $\sigma_h = 0.24$ MPa. Thus, in the performed experiments, in addition to the uniaxial pressure, the sample was exposed to a lateral pressure of approximately half the vertical pressure, which does not correspond to the conditions of the pebble stress according to Figure 1.

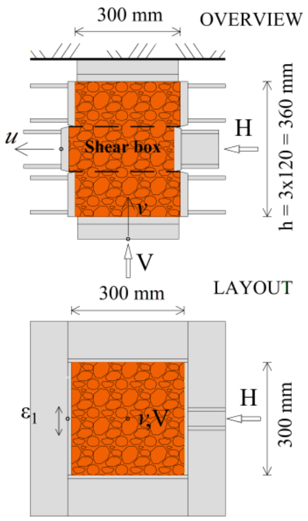

Figure 14 – *Measured quantities during direct shear testing*

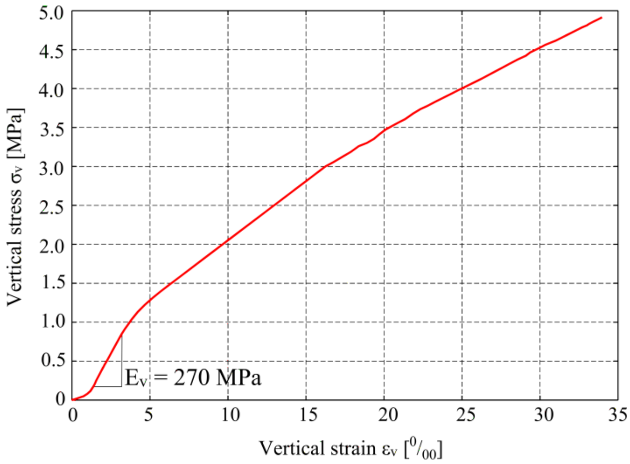

Figure 15 – *Normal stress–normal strain curve due to testing of a stone pebble in shear box subjected to normal stress only (without shear force)*

Assuming that the horizontal strain of the pebbles is completely prevented from the action of normal stress in the shear box and elastic behavior, the following expression yields

$$\varepsilon_h = \sigma_h/E_h - \nu_h \cdot \sigma_v/E_v = 0 \tag{7}$$

and:

$$\nu_h = (\sigma_h \cdot E_v)/(\sigma_v \cdot E_h) \tag{8}$$

Assuming the isotropic elastic behavior of the pebbles in the performed test with prevented lateral strain, from Equation (8) for $\sigma_v = 0.5$ MPa and $\sigma_h = 0.24$ MPa yields

$$\nu_h = \sigma_h/\sigma_v = 0.24/0.50 = 0.48 \tag{9}$$

where ν_h is very close to the so-called coefficient of resting pressure on the non-deformable vertical wall from the horizontal ground pressure. Assuming the orthotropic coefficient of the real pebble layer according to Figure 1 as $c_o = E_h/E_v = \nu_v/\nu_h = 2$, yields

$$\nu_v = 0.48/2 = 0.24 \tag{10}$$

$$E_h = 270/2 = 135\ MPa \tag{11}$$

ome results of the direct shear tests are shown hereinafter. The shear stress–horizontal displacement curve due to direct shear testing of stone pebbles subjected to different vertical stresses σ_v is presented in Figure 16. If an average shear stress τ_a is calculated as

$$\tau_a = H/(2A_n) \tag{12}$$

where H is the shear force, A_n is the net cross-sectional area of the pebble sample exposed to the vertical pressure, and if the average shear deformation γ_a is expressed as

$$\gamma_a = u/h_1 \tag{13}$$

where u is the horizontal displacement of the middle metal shear box, h_1 is its height, and the τ_a-γ_a relation shown in Figure 17 is valid.

The actual (curvilinear) and previously defined uniform distribution of shear stress in the horizontal cross-section of the pebble sample is shown in Figure 18. The resulting shear force for both of these shear-stress distributions is equal (shear stress integral on the shear surface). The normal stress–shear stress relation is presented in Figure 19. For low levels of σ_v, this relation is approximately linear, while with increasing, σ_v it is increasingly nonlinear. The slope of the normal stress–shear stress curve is the angle of internal friction of the pebbles φ, which decreases with increasing normal stress. The initial φ is approximately 48^0, which is close to the value experimentally determined by Indraratna *et al.* [2011] for similar gravel materials. For σ_v = 0, the actual shear strength of the pebbles disappears. The experimentally determined strength for this case is due to the influence of the shear box, the loading speed, and other imperfections of the experiment. Once again, it is important to note that in this experiment, the pebbles were exposed to both vertical pressure and biaxial lateral pressure of close to 50% of the vertical pressure. Such a stress state does not correspond to the actual stress state of the pebbles under the building foundation, where they are predominantly exposed to uniaxial pressure and shear.

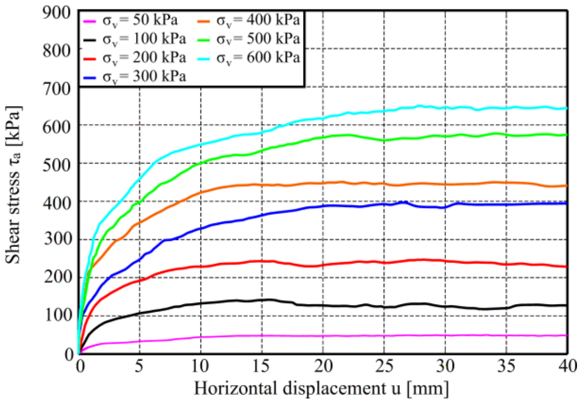

Figure 16 – *Shear stress–horizontal displacement curve due to direct shear testing of stone pebbles subjected to different vertical stresses σ_v*

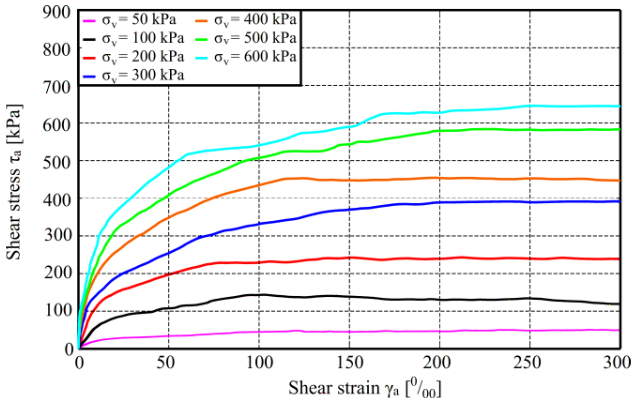

Figure 17 – *Shear stress–shear strain curve due to direct shear testing of stone pebbles subjected to different vertical stresses σ_v*

Therefore, the relation σ_v-τ according to Figure 19 does not apply to the problem considered in Figure 1. The actual σ_v-τ relation for this problem is closer to the adopted diagram according to Figure 11 and is planned to be experimentally determined soon by a different approach. The bulk density of the pebbles compacted to MS = 30 MPa was γ_0 = 1680 kg/m^3.

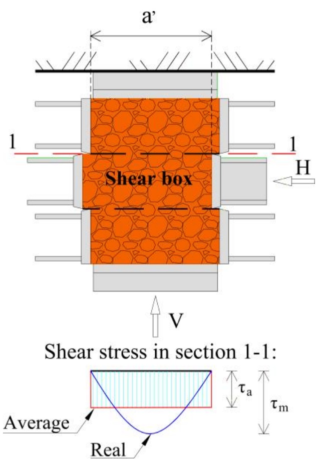

Figure 18 – *Shear stress distribution in section 1-1*

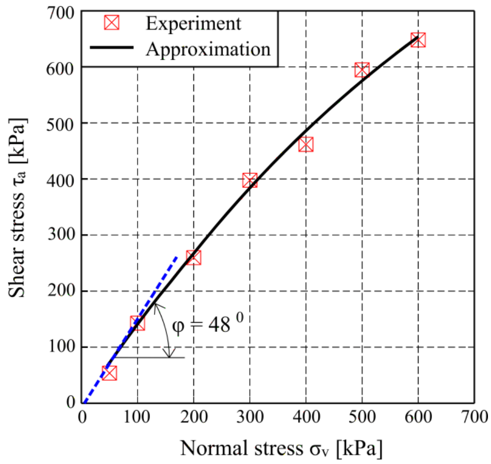

Figure 19 – *Shear stress–normal stress relation and frictional angle φ derived from direct shear testing*

4.2 Some parameters of the foundation-pebble layer coupling surface

The friction angle φ_c of the pebble layer subjected to different vertical stresses against a smooth prefabricated foundation interface was measured through experimental testing, as shown in Figure 20. A concrete prism with ground plan dimensions of 0.5 m x 0.5 m with variable additional weight at the top was adopted. The normal stress–shear stress relation derived from the previously mentioned experimental setup is presented in Figure 21. Based on the experimental results, φ_c = 27^0 was adopted. Clearly, there is a large difference between φ_c and φ = 48^0.

The values of the parameters of the foundation-pebble layer coupling surface were calculated using the mechanical parameters of the pebble layer as

$$\tau_{0,c}=(\varphi_c/\varphi_0)\tau_m \tag{13}$$

$$G_c=(\varphi_c/\varphi_0)G \tag{14}$$

$$\gamma_{u,c}=(\varphi_0/\varphi_c)\gamma_u \tag{15}$$

where τ_m, G, γ_u, φ refer to the pebble layer, and $\tau_{0,c}$, G_c, $\gamma_{u,c}$, φ_c to the foundation-pebble layer coupling surface behavior, respectively.

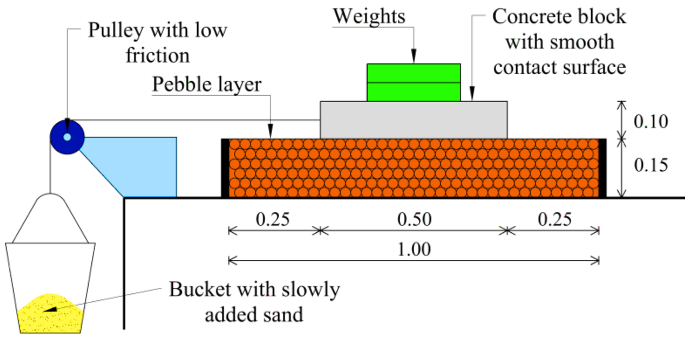

Figure 20 – *Experimental setup: rigid concrete block with smooth contact surface designed to slide against the pebble layer to determine friction angle φ_c*

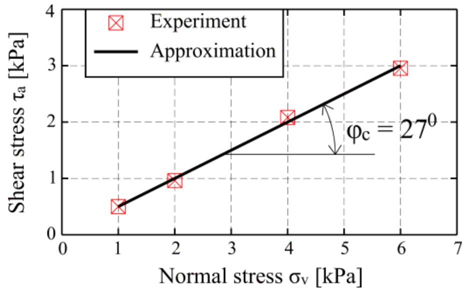

Figure 21 – *Normal stress–shear stress relation for experimental setup according to Figure 20*

5 Verification of the presented numerical model

The numerical model for dynamic analysis of planar structures presented in Section 3, with the developed constitutive models for the stone pebble layer and the foundation-layer contact surface, was verified using shake-table tests of simple structural models based on an aseismic layer of stone pebbles. In this study, only the model of a very stiff building M_1 and the model of a stiff building M_2 [Banović *et al.*, 2020b] are considered, whose data are shown in Figure 22. The model column is made of a square cross-section steel tube, with a rigid concrete block of m = 1000 kg on the column top. The models have a concrete foundation, dimensions 1.2 m x 0.7 m x 0.3 m, which is based on an aseismic layer with the following characteristics: thickness h_p = 0.3 m, fraction ϕ_b=16-32 mm, compaction MS = 30 MPa and humidity h_m = 10%. A more detailed description of the conducted experimental tests can be found in [Banović *et al.*, 2020b]. The models were exposed to horizontal accelerations of four accelerograms (artificial accelerogram-AA, accelerogram Petrovac-AP, accelerogram Ston-AS, and accelerogram Banja Luka-ABL), as shown in Figure 23.

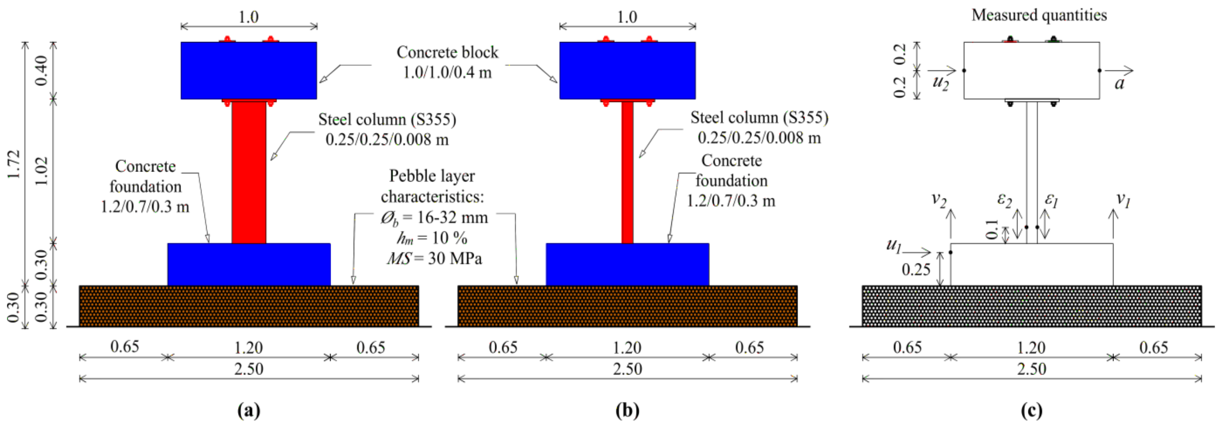

Figure 22 – *Considered models previously tested by shake-table: (a)Very stiff model M_1, (b) Stiff model M_2, (c) Measured quantities during shake-table testing*

All accelerograms were scaled to equal peak ground acceleration (PGA) = 0.3 g. An artificial accelerogram-AA was created to match the elastic response spectrum according to Eurocode 8 [2004], for earthquake type 1 and soil type A. The AA is generated using SIMQKE software [1976], as a superposition of sine functions. Time-histories of AP, AS, and ABL earthquakes were acquired from the European Strong-Motion Database [Ambraseys *et al.*, 2001]. The presented numerical model was verified using a simulation of 10 conducted experimental tests (Table 1). The spatial discretization of the models is presented in Figure 24.

Table 1- *Performed numerical simulations of experiments*

Excitation	Model M_1	Model M_2	
AA	+	+	*One-time base excitation with PGA = 0.3 g*
AP	+	+	
AS	+	+	
ABL	+	+	
AA	+	+	*Successive application of AA excitation until model collapse*

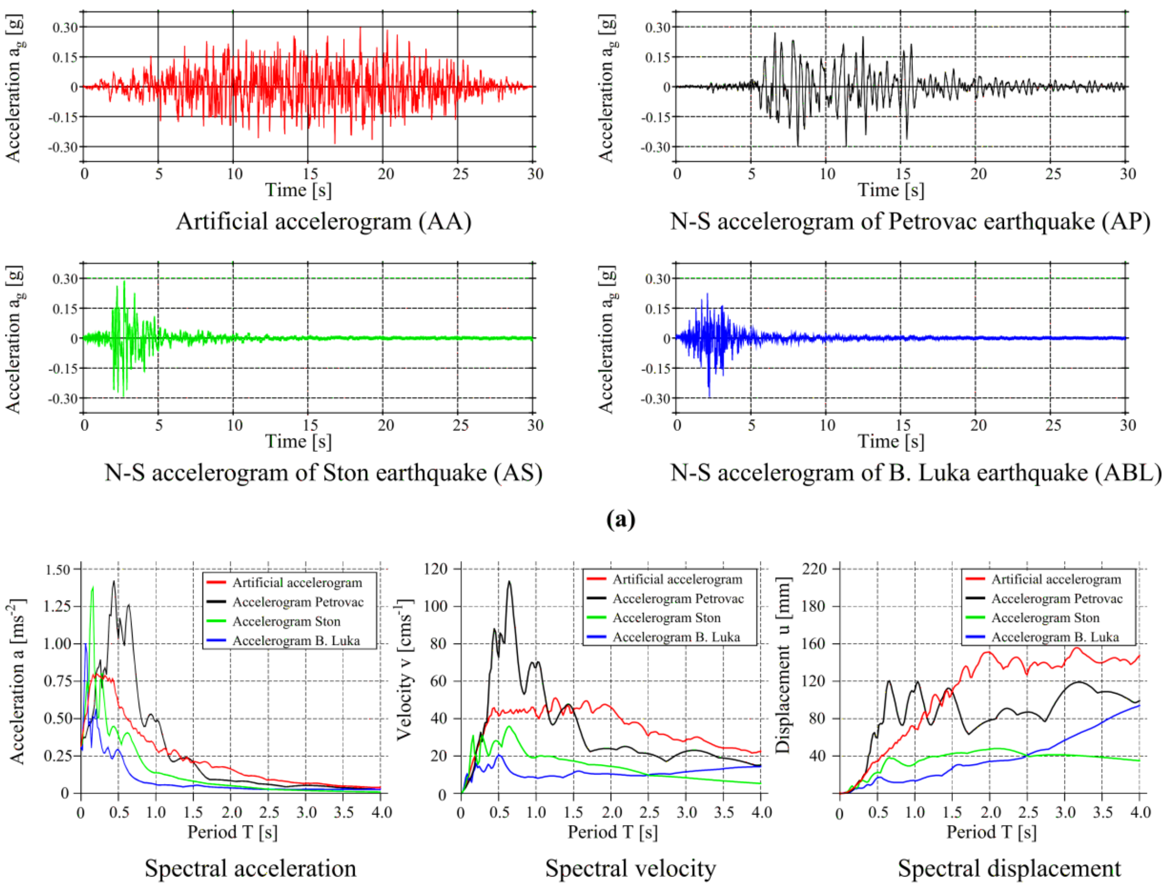

Figure 23 – *Applied horizontal base excitations: (a) Accelerograms, (b) Elastic response spectrum*

Thin contact elements were used at the foundation-pebble layer contact surface. A mesh of regular finite elements was used. It should be noted that the concrete block at the top of the column and the concrete foundation are rigid. Therefore, these elements are simulated with elastic behavior and extreme strengths to simplify and shorten dynamic analyses. The parameters of steel, stone pebbles, and contact element constitutive models are presented in Table 2. The dominant part of energy dissipation (damping) was modeled through the adopted nonlinear constitutive models of materials and the nonlinear model of geometry (large displacements). The rest of the energy dissipation that cannot be simulated by adopted nonlinearities was modeled via Rayleigh viscous dumping. In the performed numerical simulations of experimental tests with lower PGA levels, the viscosity damping coefficient was not included. For tests with successive application of excitation until model failure, this coefficient was taken as 1.0%.

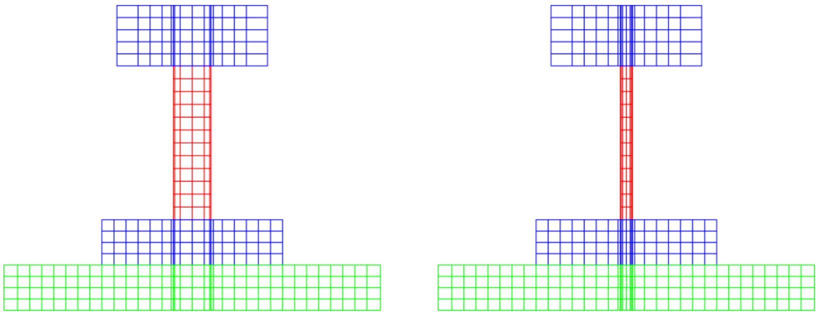

(a) **(b)**

Figure 24 – *Spatial discretization by finite elements: (a) M_1 model, (b) M_2 model*

Table 2- *Adopted basic parameters of steel, stone pebbles, and contact elements constitutive models*

Steel				
E (GPa)	$f_{c,\,steel}$ (MPa)	$f_{t,\,steel}$ (MPa)	ν_{steel}	ε_{steel} [$^0/_{00}$]
200	520	520	0.3	20

Stone pebbles											
E_v (MPa)	E_h (MPa)	f_v (MPa)	f_h (MPa)	τ_m (MPa)	ν_v	ν_h	$\varepsilon_{u,v}$ [$^0/_{00}$]	$\varepsilon_{u,h}$ [$^0/_{00}$]	G (MPa)	γ_u [$^0/_{00}$]	φ [^{0}]
270	135	6.0	3.0	1.8	0.24	0.48	20	40	64.3	100	48

Contact element: foundation-pebble layer coupling surface							
E_c (MPa)	$f_{v,c}$ (MPa)	$\tau_{m,c}$ (MPa)	ν_c	$\varepsilon_{u,c}$ [$^0/_{00}$]	G_c (MPa)	$\gamma_{u,c}$ [$^0/_{00}$]	φ_c [^{0}]
270	6.0	1.01	0.24	20	36.17	177	27

Only some results of the performed dynamic analyses are presented, and these are discussed below. A comparison of the time sequence of experimentally determined and numerically obtained results of measured accelerations, displacements, and strains for AA excitation at PGA = 0.3 g is presented in Figure 25. This sequence is quite identical for both models as well as the correlation of the measured peak values (see Table 3). Deviations in the "frequencies" of the time response of quantities a, u_2, ε_1 between the experiment and the numerical model is due to the difference in their stiffness and material properties, model parameters (spatial and temporal discretization, convergence criterion, etc.), and due to other influential parameters. It should be noted that the numerical model obtains a slightly stiffer construction of the physical model, resulting in slightly higher accelerations and strains and smaller displacements. This is probably due to the inadequacy of the adopted constitutive models of materials, overestimated values of strengths and modulus of elasticity, design parameters, etc.

Although the stresses on the bottom of the steel column are in the elastic region, owing to the nonlinear behavior of the seismic layer and the nonlinear behavior at the foundation-seismic isolation coupling surface, the obtained numerical results can be considered acceptable, especially the peak values according to Table 3.

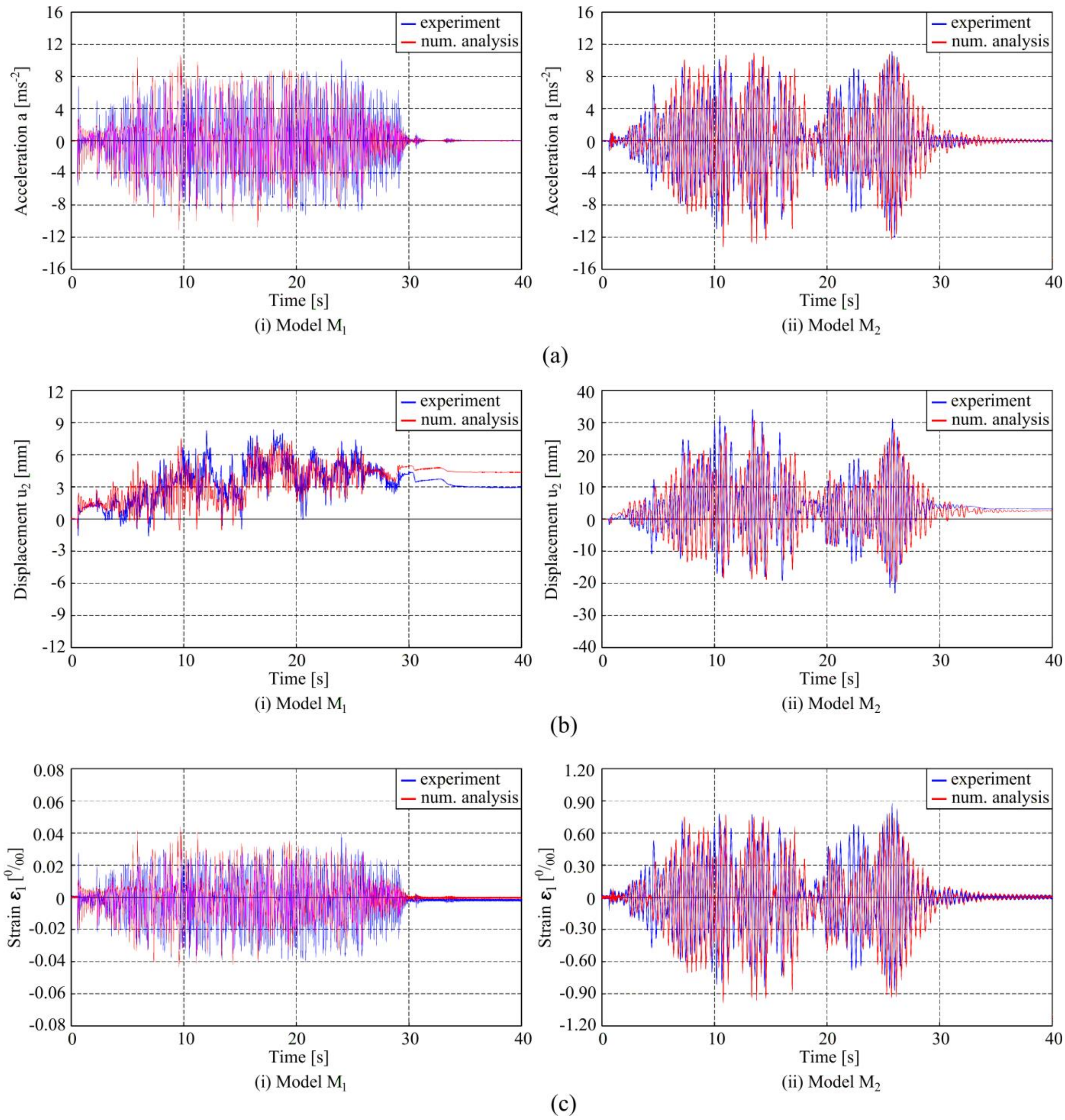

Figure 25 – *Comparison of experimentally determined and numerically obtained results for applied AA accelerogram (PGA = 0.3 g): (a) Horizontal acceleration of the mass at the column top, (b) Horizontal displacement of the mass at the column top, (c) Vertical strain on the right bottom side of the steel column*

A comparison of the time history of the experimental and numerical results for a, u_2, ε_1 under the action of an ABL accelerogram with PGA = 0.3 g is shown in Figure 26. A good agreement between the experimental and numerical results can also be spotted, similar to those in Figure 25 and Table 3 for the AA accelerogram.

A comparison of the peak values of measured quantities determined using the experimental model and calculated using the presented numerical model for applied excitations at PGA = 0.3 g is presented in Table 3.

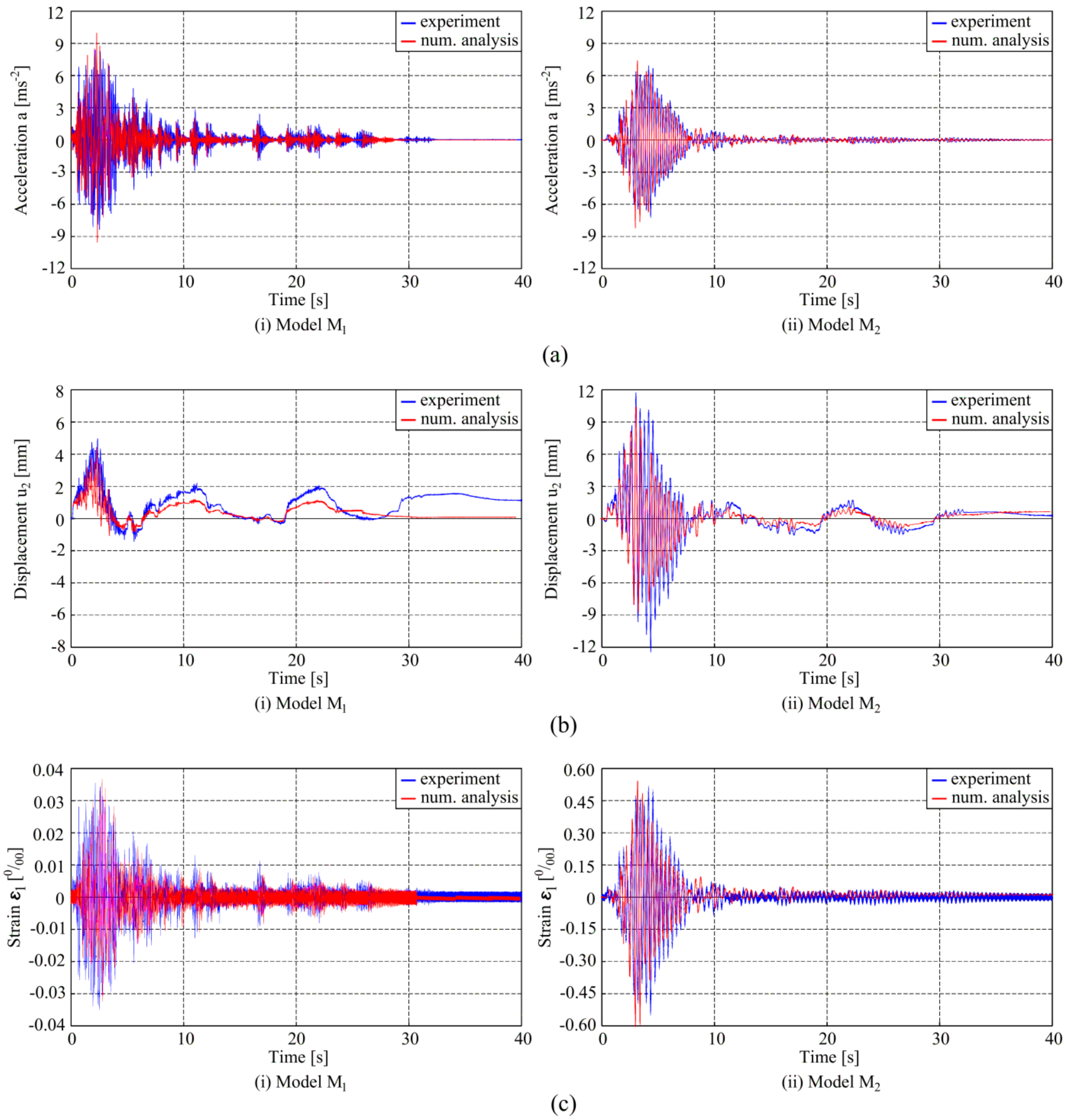

Figure 26 – *Comparison of experimentally determined and numerically obtained results for applied ABL accelerogram (PGA = 0.3 g): (a) Horizontal acceleration a of the mass at the column top, (b) Horizontal displacement u_2 of the mass at the column top, (c) Vertical strain ε_1 on the right bottom side of the steel column*

It can be observed that for the short predominant period, impact accelerograms AS and ABL, the deviations of the experimental and numerical values are slightly larger than those for the accelerograms with a larger predominant period (AA and AP). Nevertheless, these deviations can still be considered within acceptable limits.

A comparison of the artificial accelerogram PGA at which the physical and numerical models collapsed, with a successive increase in the acceleration $\Delta a_{g,\ max}$ = 0.05 g, is presented in Table 4. It can be noted that the PGA values at the collapse of the experimentally tested model are slightly higher than the values at the collapse of the numerical model. Thus, in the considered examples, the numerically obtained PGA values are conservative in relation to the experiment, which may not be the case in many other examples. The difference in the experimental and numerical values of PGA is relatively small, especially when we consider that numerous nonlinearities in the structure progressively occur before its failure.

Table 3- *Comparison of some peak values of experimentally determined and numerically obtained results for one-time base excitation (PGA = 0.3 g)*

	AA			AP			AS			ABL		
Model M_1	Exp.	Num.	Rel. error [%]	Exp.	Num.	Rel. error [%]	Exp.	Num.	Rel. error [%]	Exp.	Num.	Rel. error [%]
a [ms^{-2}]	10.18	11.17	9.7	9.90	10.74	8.4	10.73	12.34	15	8.41	9.96	18.4
ε_1 [$^0/_{00}$]	0.040	0.043	7.5	0.040	0.042	5.0	0.042	0.047	11.9	0.030	0.035	16.7
u_2 [mm]	7.95	7.52	5.7	5.20	4.81	7.5	7.00	5.97	17.2	5.00	4.42	13.1
Model M_2												
a [ms^{-2}]	11.86	13.17	10.0	14.17	15.89	12.1	7.89	8.86	10.9	7.22	9.24	14.1
ε_1 [$^0/_{00}$]	0.870	0.962	11.1	1.020	1.121	9.9	0.587	0.660	12.4	0.537	0.606	12.8
u_2 [mm]	33.75	30.7	9.4	40.4	37.1	8.2	17.5	15.1	15.9	12.5	10.41	16.7

Table 4- *Comparison of the PGA of the artificial accelerogram at which the physical and numerical model collapsed*

	Model M_1		Model M_2	
	Exp.	Num.	Exp.	Num.
PGA [g]	0.55	0.50	0.45	0.40

6 Conclusions

This paper briefly presents the previously developed numerical model for the dynamic analysis of planar concrete, steel, and masonry structures based on FEM. The model was then extended with developed constitutive models of the stone pebble aseismic layer behavior and the foundation-pebble layer coupling surface behavior. The numerical model is based on a relatively small number of parameters and is intended for practical application. The verification of the numerical model was performed on several previously performed shake-table tests of simple models of very stiff and stiff building on an aseismic layer of pebbles, with four different earthquake accelerograms. A good agreement was observed between the experimental and numerical values of the measured accelerations, displacements, and strains/stresses, both for lower PGA levels and for structural collapse at higher PGA levels. However, further verification of this model is needed, as well as its improvement.

7 Acknowledgements

This work has been fully supported by the Croatian Science Foundation under the project *"Seismic base isolation of a building by using natural materials - shake table testing and numerical modeling*" [IP-06-2016-5325]. The work of doctoral student Ivan Banović has been fully supported by the *"Young researchers' career development project – training of doctoral students"* of the Croatian Science Foundation funded by the European Union from the European Social Fund. The authors are grateful for the support.

References

Ambraseys, N., Smit, P., Sigbjornsson, R., Suhadolc, P., Margaris, M. (2001). EVR1-CT-1999-40008, European Commission, Directorate-General XII, Environmental and Climate Programme, Brussels, Belgium

Amendola, A., Carpentieri, G., Feo, L., Fraternali, F. (2016a). Bending dominated response of layered mechanical metamaterials alternating pentamode lattices and confinement plates. Composite Structures. 157, 71-77.

Amendola, A., Smith, C.J., Goodall, R., Auricchio, F., Feo, L., Benzoni, G., Fraternali, F. (2016b). Experimental response of additively manufactured metallic pentamode materials confined between stiffening plates. Composite Structures. **142**, 254-262.

Anastasopoulos, I., Kourkoulis, R., Gelagoti, F., Papadopoulos, E. (2012b). Rocking response of SDOF systems on shallow improved sand: An experimental study. Soil Dynamics and Earthquake Engineering. **40**: 15-33.

Anastasopoulos, I., Loli, M., Georgarakos, T., Drosos, V. (2012a). Shaking table testing of rocking-isolated bridge pier on sand. Journal of Earthquake Engineering. **17**(1): 1–32.

Avossa, A. M., Pianese, G. (2017). Damping effects on the seismic response of base-isolated structures with LRB devices. Ingegneria Sismica. **34**(2): 3-30.

Azinović, B., Kilar, V., Koren, D. (2014). The seismic response of low-energy buildings founded on a thermal insulation layer –a parametric study. Engineering Structures. **81**: 398-411.

Azinović, B., Kilar, V., Koren, D. (2016). Energy-efficient solution for the foundation of passive houses in earthquake-prone regions. Engineering Structures. **112**: 133-145.

Azzam, W., Ayeldeen, M., El Siragy, M. (2018). Improving the structural stability during earthquakes using in-filled trench with EPS geofoam—numerical study. Arabian Journal of Geosciences. **11**(14): 395.

Baloević, G., Radnić, J., Grgić, N. (2019). Numerical model for dynamic analysis of masonry-infilled steel and concrete frames. Materialwissenschaft und Werkstofftechnik. **50**(5): 519-532.

Baloević, G., Radnić, J., Grgić, N., Matešan, D., Smilović, M. (2016b). Numerical model for nonlinear analysis of composite concrete-steel-masonry bridges. Coupled Systems Mechanics. **5**(1): 1-20.

Baloević, G., Radnić, J., Matešan, D., Grgić, N., Banović, I. (2016a). Comparison of Developed Numerical Macro and Micro Masonry Models for Static and Dynamic Analysis of Masonry-infilled Steel Frames. Latin American Journal of Solids and Structures. **13**(12), 2251-2265.

Bandyopadhyay, S., Sengupta, A., Reddy, G. R. (2015). Performance of sand and shredded rubber tire mixture as a natural base isolator for earthquake protection. Earthquake Engineering and Engineering Vibration. **14**(4): 683–693.

Banović, I., Radnić, J., Grgić, N. (2018b). Shake table study on the efficiency of seismic base isolation using natural stone pebbles. Advances in Materials Science and Engineering, Article ID 1012527, 20 pages

Banović, I., Radnić, J., Grgić, N. (2019). Geotechnical seismic isolation system based on sliding mechanism using stone pebble layer: shake-table experiments. Shock and Vibration, Article ID 9346232, 26 pages

Banović, I., Radnić, J., Grgić, N. (2020a). Effect of structural stiffness on the efficiency of seismic base isolation using layers of stone pebbles. Ingegneria Sismica, **37**(2): 66-91.

Banović, I., Radnić, J., Grgić, N. (2020b). Foundation size effect on the efficiency of seismic base isolation using a layer of stone pebbles. Earthquakes and Structures. **19**(2): 103-117.

Banović, I., Radnić, J., Grgić, N., Matešan, D. (2018a). The use of limestone sand for the seismic base isolation of structures. Advances in Civil Engineering. Article ID 9734283, 12 pages

Brunet, S., de la Llera, J. C., Kausel, E. (2016). Non-linear modeling of seismic isolation systems made of recycled tire-rubber. Soil Dynamics and Earthquake Engineering. **85**: 134–145.

Calvi, P. M., Moratti, M., Calvi, G. M. (2016). Seismic Isolation Devices Based on Sliding Between Surfaces with Variable Friction Coefficient. Earthquake Spectra. **32**(4): 2291-2315.

Castaldo, P., Ripani, M. (2017). Optimal design of single concave sliding bearings for isolated structures considering intermediate isolation degrees. Ingegneria Sismica. **34** (5): 5-24.

Chen, X., Xia, X., Zhang, X., Gao, J. (2020). Seismic performance and design of bridge piers with rocking isolation. Structural Engineering and Mechanics. **73**(4): 447-454.

Chung, Y. L., Du, L. J., Pan, H. H. (2019). Performance evaluation of a rocking steel column base equipped with asymmetrical resistance friction damper. Earthquakes and Structures. **17**(1): 49-61.

De Domenico, D., Ricciardi, G., Infanti, S., Benzoni, G. (2019). Frictional Heating in double curved surface sliders and its effects on the hysteretic behavior: an experimental study. Frontiers in Built Environment. **5**(74)

Dhanya, J. S., Boominathan, A., Subhadeep Banerjee. (2019). Performance of Geo-Base Isolation System with Geogrid Reinforcement. International Journal of Geomechanics. **19**(7).

Dhanya, J. S., Boominathan, A., Subhadeep Banerjee. (2020). Response of low-rise building with geotechnical seismic isolation system. Soil Dynamics and Earthquake Engineering. **136**

Doudoumis, I., Papadopoulos, P.,Papaliangas, T. (2002). Low-cost base isolation system on artificial soil layers with low shearing resistance. Proceedings of the 12th European Conference on EE, UK

EN 1998-1:2004 (2004). Eurocode 8: Design of Structures for Earthquake Resistance-Part 1: General Rules, Seismic Actions and Rules for Buildings, European Committee for Standardization, Belgium

Fabbrocino, F., Amendola, A., Benzoni, G., Fraternali, F. (2016). Seismic application of pentamode lattices. Ingegneria Sismica. **1**:62-71.

Forcellini, D. (2017). Assessment on geotechnical seismic isolation (GSI) on bridge configurations. Innovative Infrastructure Solutions **2**(1), 9 pages.

Forcellini, D. (2020). Assessment of Geotechnical Seismic Isolation (GSI) as a Mitigation Technique for Seismic Hazard Events. Geosciences. **10**, 222.

Fraternali, F., Amendola, A., Benzoni, G. (2018). Innovative seismic isolation devices based on lattice materials: A review. Ingegneria Sismica. **4**:93-113.

Hadad, H. A, Calabrese, A., Strano, S., Serino, G. (2017). A base isolation system for developing countries using discarded tyres filled with elastomeric recycled materials. Journal of Earthquake Engineering. **21**(2): 246-266.

Hernández, E., Palermo, A., Granello, G., Chiaro, G., Banasiak, L. (2020). Eco-rubber Seismic-Isolation Foundation Systems: A Sustainable Solution for the New Zealand Context. Structural Engineering International. 1-9.

Hughes, T. J. R., Pister, K. S., Taylor, R. L. (1979). Implicit-explicit finite elements in nonlinear transient analysis. Computer Methods in Applied Mechanics and Engineering. **17–18**: 159–182.

Indraratna, B., Ngo, T., Rujikiatkamjorn, C. (2011). Behavior of geogrid-reinforced ballast under various levels of fouling. Geotextiles and Geomembranes. **29**(3): 313-322.

Kalpakcı, V., Bonab, A. T., Özkan, M. Y., Gülerce, Z. (2018). Experimental evaluation of geomembrane/geotextile interface as base isolating system. Geosynthetics International. **25**(1), 1-11.

Karatzia, X., Mylonakis, G. (2017). Geotechnical seismic isolation using eps geofoam around piles. 6th International Conference on Computational Methods in Structural Dynamics and EE, Greece

Kelly, J. (1986). Aseismic base isolation: review and bibliography. Soil Dynamics and Earthquake Engineering. **5**(4), 202-216.

Koren, D., Kilar, V. (2016). Seismic vulnerability of reinforced concrete building structures founded on an XPS layer. Earthquakes and Structures. **10**(4), 939 -963.

Kuvat, A., Sadoglu, E. (2020). Dynamic properties of sand-bitumen mixtures as a geotechnical seismic isolation material. Soil Dynamics and Earthquake Engineering. **132**, 106043

Lomiento, G., Bonessio, N., Benzoni, G. (2013). Concave sliding isolator's performance under multi-directional excitation. Ingegneria Sismica. **30**:17-32.

Makris, N. (2014). A half-century of rocking isolation. Earthquakes and Structures. **7**(6), 1187-1221.

Makris, N. (2018). Seismic isolation: early history. Earthquake Engineering and Structural Dynamics. **48** (2), 269-283.

Mavronicola E., Komodromos P., Charmpis D. C. (2010). Numerical investigation of potential usage of rubber–soil mixtures as a distributed seismic isolation approach. Proceedings of the 10th International Conference on Computational Structures Technology, Valencia, Spain

Murillo, C., Thorel, L., Caicedo, B. (2009). Ground vibration isolation with geofoam barriers: centrifuge modelling. Geotextiles and Geomembranes. **27**(6), 423-434.

Naeim, F., Kelly, J. M. (1999). Design of seismic isolated structures: From theory to practice. John Wiley & Sons, Inc., New York.

OECD (2008) Costs of Inaction of Environmental Policy Challenges Report ENV/EPOC(2007)17/REV2

Panjamani, A., Devarahalli Ramegowda, M., Divyesh, R. (2015). Low cost damping scheme for low to medium rise buildings using rubber soil mixtures. Japanese Geotechnical Society Special Publication. **3**(2), 24–28.

Patil, S. J., Reddy, G. R., Shivshankar, R., Babu, R., Jayalekshmi, B. R., Kumar, B. (2016). Seismic base isolation for structures using river sand. Earthquakes and Structures. **10**(4), 829-847.

Petrone, G., Ferrentino, T., Alfano, G. (2017). Influence of PGA/PGV ratio on the seismic reliability of base-isolated system with FPS. Ingegneria Sismica. **34**(3): 39-62.

Pistolas, G. A., Pitilakis, K., Anastasiadis, A. (2020). A numerical investigation on the seismic isolation potential of rubber/soil mixtures. Earthquake Engineering and Engineering Vibration. **19**: 683–704.

Pitilakis, K., Karapetrou, S., Tsagdi, K. (2015). Numerical investigation of the seismic response of RC buildings on soil replaced with rubber–sand mixtures. Soil Dynamics and Earthquake Engineering. **79**: 237–252.

Radnić, J., Grgić, N., Matešan, D., Baloević, G. (2015). Shake table testing of reinforced concrete columns with different layout size of foundation. Materialwissenschaft und Werkstofftechnik. **46**(4-5): 348–367.

Radnić, J., Harapin, A., Matešan, D., Trogrlić, B., Smilović, M., Grgić, N., Baloević, G. (2011). Numerical Model for Analysis of Masonry Structures. Gradjevinar, **63**(6): 529-546.

Radnić, J., Markić, R., Grgić, N., Glibić, M., Banović, I. (2016). Comparison of numerical models for nonlinear static analysis of planar concrete frames based on 1D and 2D finite elements. Materialwissenschaft und Werkstofftechnik. **47**(5-6): 369-581.

Radnić, J., Matešan, D., Harapin, A., Smilović, M., Grgić, N. (2012). Numerical model for static and dynamic analysis of masonry structures. Mechanics and Properties of Composed Materials and Structures. Advanced Structured Materials, 1–33, Springer-Verlag, Berlin, Germany

SIMQKE (SIMulation of earthQuaKE ground motions) (1976). http://gelfi.unibs.it/software/simqke/simqke_gr.htm

Smilović Zulim, M., Radnić, J. (2020). Anisotropy Effect of Masonry on the Behaviour and Bearing Capacity of Masonry Walls. Advances in Materials Science and Engineering. 2020, 5676901

Smilović Zulim, M., Radnić, J., Grgić, N., Baloević, G. (2018). Effect of anisotropy of masonry on the behaviour of unreinforced and confined masonry walls under ground motion. Engineering Design Applications. Heidelberger, Springer, Cham, 173-183.

Smilović Zulim, M., Radnić, J., Harapin, A. (2019). Shear effect on seismic behaviour of masonry walls. Materialwissenschaft und Werkstofftechnik. **50**(5), 565-579.

Sorrentino, L., Masiani, R., Decanini, L. D. (2006). Overturning of rocking rigid bodies under transient ground motions. Structural Engineering and Mechanics. **22**(3), 293-310.

Sorrentino, L., Masiani, R., Griffith, M. C. (2008). The vertical spanning strip wall as a coupled rocking rigid body assembly. Structural Engineering and Mechanics. **29**(4): 433-453.

Tehrani, F. M., Hasani, A. (1996). Behaviour of Iranian low rise buildings on sliding base to earthquake excitation. Proceedings of the 11th World Conference on Earthquake Engineering, Paper 1433, Acapulco, Mexico

Titirla, M. D., Katakalos K., Zuccaro G., Fabbrocino F. (2017). On the mechanical modeling of an innovative energy dissipation device. Ingegneria Sismica. **34**(2): 126-137.

Tsang, H. H. (2008). Seismic isolation by rubber-soil mixtures for developing countries. Earthquake Engineering & Structural Dynamics. **37**(2): 283–303.

Tsang, H. H. (2009). Geotechnical seismic isolation. Earthquake Engineering: New Research. 55–87, Nova Science Publishers Inc., New York, NY, USA

Tsang, H. H., Lo, S. H., Xu, X., Neaz Sheikh, M. (2012). Seismic isolation for low-to-medium-rise buildings using granulated rubber-soil mixtures: numerical study. Earthquake Engineering & Structural Dynamics. **41**(14): 2009–2024.

Tsang, H. H., Pitilakis, K. (2019). Mechanism of geotechnical seismic isolation system: Analytical modeling. Soil Dynamics and Earthquake Engineering. **122**: 171-184.

Tsiavos, A., Alexander, N. A., Diambra, A., Ibraim, E., Vardanega, P. J., Gonzalez-Buelga, A., Sextos A. (2019a). A sand-rubber deformable granular layer as a low-cost seismic isolation strategy in developing countries: experimental investigation. Soil Dynamics and Earthquake Engineering. 125.

Tsiavos, A., Alexander, N. A., Sextos, A. (2019b). Numerical investigation of the sliding response of flexible structures founded on a deformable granular layer. 2nd International Conference on Earthquake Engineering and Post Disaster Reconstruction Planning, Bhaktapur, Nepal

Tsiavos, A., Haladij, P., Sextos, A., Alexander, N. A. (2020b). Analytical investigation of the effect of a deformable sliding layer on the dynamic response of seismically isolated structures. Structures. **27**: 2426-2436.

Tsiavos, A., Sextos, A., Stavridis, A., Dietz, M., Dihoru, L., Alexander, N. A. (2020a). Large-scale experimental investigation of a low-cost PVC 'sand-wich' (PVC-s) seismic isolation for developing countries. Earthquake Spectra.

Xiong, W., Li, Y. (2013). Seismic isolation using granulated tiresoil mixtures for less-developed regions: experimental validation. Earthquake Engineering & Structural Dynamics. **42**(14), 2187-2193.

Xiong, W., Yan, M. R., Li, Y. Z. (2014). Geotechnical Seismic Isolation System - Further Experimental Study. Applied Mechanics and Materials. **580-583**: 1490-1493.

Yegian, M. K., Kadakal, U. (2004). Foundation isolation for seismic protection using a smooth synthetic liner. Journal of Geotechnical and Geoenvironmental Engineering. **130**(11): 1121–1130.

Yegian, M. K., Lahlaf, A. M. (1992). Geomembranes as base isolation. Geotechnical Fabrics Report. **10**(6): 17-21.

Zhao, X., Zhang, Q., Zhang, Q., He, J. (2016). Numerical study on seismic isolation effect of gravel cushion. Proceedings of the 7th International Conference on DEM. **188**: 1055-1063., Dalian, China

Zorn, M. (2018). Natural Disasters and Less Developed Countries: Nature, Tourism and Ethnicity as Drivers of (De)Marginalization. Perspectives on Geographical Marginality, vol 3. Springer, Cham.

ingegneria sismica
International Journal of Earthquake Engineering
Anno XXXVIII – Num.1 - 2021

NUMERICAL MODEL FOR DYNAMIC ANALYSIS OF STRUCTURES WITH SEISMIC BASE ISOLATION USING A LAYER OF STONE PEBBLES

Ivan Banović[1], Jure Radnić[1], Nikola Grgić[1]

[1]University of Split, Faculty of Civil Engineering, Architecture and Geodesy, Split, Croatia

SUMMARY: *Questo articolo presenta un modello numerico per l'analisi dinamica di strutture planari con isolamento sismico alla base utilizzando uno strato pietrame. Dopo una breve presentazione del modello numerico sviluppato in precedenza per l'analisi strutturale, vengono presentati il modello costitutivo sviluppato per lo strato di pietrame e il modello costitutivo per la simulazione della superficie di accoppiamento strato di fondazione-isolamento. Il modello si basa su un numero relativamente piccolo di parametri, alcuni dei quali sono stati determinati sperimentalmente. Il modello numerico è stato verificato simulando i test su tavola vibrante eseguiti su semplici modelli strutturali basati su uno strato antisismico di pietrame, ed è stata osservata una buona concordanza tra i risultati sperimentali e numerici. Infine, vengono delineate ulteriori verifiche e miglioramenti dei modelli costitutivi presentati.*

KEYWORDS: *seismic base isolation, stone pebble layer, numerical model, constitutive model*

Corresponding author: Ivan Banović, PhD; University of Split, Faculty of Civil Engineering, Architecture and Geodesy, Croatia.
Email: ivan.banovic@gradst.hr